

# Achieving Centimeter-Accuracy Indoor Localization on WiFi Platforms: A Frequency Hopping Approach

Chen Chen, *Student Member, IEEE*, Yan Chen, *Senior Member, IEEE*, Yi Han, *Member, IEEE*, Hung-Quoc Lai, *Member, IEEE*, and K. J. Ray Liu, *Fellow, IEEE*

**Abstract**—Indoor positioning systems (IPSs) are attracting more and more attention from the academia and industry recently. Among them, approaches based on WiFi techniques are more favorable since they are built upon the WiFi infrastructures available in most indoor spaces. However, due to the bandwidth limit in mainstream WiFi systems, the IPS leveraging WiFi can hardly achieve centimeter localization accuracy under strong nonline-of-sight (NLOS) conditions which is common for indoor environment. In this paper, to achieve the centimeter-level accuracy, we present a WiFi-based IPS that exploits the frequency diversity via frequency hopping. In the offline phase, the system collects channel frequency responses (CFRs) from multiple channels and from a number of locations-of-interest. Then, the CFRs are post-processed to mitigate the synchronization errors as well as interference from other WiFi networks. Then, using bandwidth concatenation, the CFRs from multiple channels are combined into location fingerprints which are stored into a local database. During the online phase, CFRs are formulated into the location fingerprint and is compared against the fingerprints in the database via the time-reversal resonating strength (TRRS). Finally, the IPS determines the location according to the TRRS. Extensive experiment results demonstrate a perfect centimeter-level accuracy in an office environment with strong NLOS using only one pair of single-antenna WiFi devices.

**Index Terms**—Channel frequency response (CFR), indoor localization, time-reversal resonating strength (TRRS), WiFi.

## I. INTRODUCTION

GLOBAL Positioning System (GPS) is an outdoor positioning system that provides real-time location information under all weather conditions near the Earth's surface, as long as there exists an unobstructed line-of-sight (LOS) from the device to at least four GPS satellites [1]. On the other hand, accurate indoor localization is highly desirable, since nowadays people spend much more time indoor than outdoor. A high accuracy indoor positioning system (IPS) can enable a wide variety of applications, e.g., providing museum guides

to tourists by localizing their exact locations [2], or supplementing users with location information in shopping malls [3]. Unfortunately, the GPS signal can be too weak to be useful in indoor spaces due to the severe attenuation of obstacles as well as scattering in the presence of a large number of reflectors.

Many research efforts have been devoted to the development of accurate and robust IPSs. According to the technologies adopted, these IPSs can be further classified into two classes, i.e., ranging-based and fingerprint-based [4]. For the ranging-based methods, at least three anchors are deployed into the indoor environment to triangulate the device through measuring the relative distances between the device to the anchors. The distances are generally obtained from other measurements, e.g., received signal strength indicator (RSSI), time of arrival (ToA), time of flight (ToF), and angle of arrival (AoA). RSSI-based ranging methods [5]–[7] utilizes the path-loss model to derive the distance and can typically achieve an accuracy of 1–3 m on average under LOS scenarios, while ToA-based ranging methods retrieve the ToA of the first arrived multipath component from the channel impulse response (CIR). To achieve a fine timing resolution, ToA-based methods require a large bandwidth, which is achievable with ultra-wideband techniques that lead to an accuracy of 10–15 cm in an LOS setting [8], [9]. Vasisht *et al.* [10] presented a decimeter-level localization using a single WiFi access point (AP). They utilize frequency hopping to acquire the channel frequency response (CFR), a fine-grained information that depicts the propagation of electromagnetic waves and thus portrays the environment with high granularity. Leveraging the nonuniform discrete Fourier transform, they recover the time-domain CIR and use the time delay of the dominant peak of the profile as the ToF measurement. However, in a strong nonline-of-sight (NLOS) environment, the dominant peak of CIR does not necessarily characterize the direct path between the WiFi devices which leads to an increased localization error. The AoA-based schemes proposed in [11] and [12] have the same issue that incurs accuracy degradation in a complicated NLOS indoor environment.

On the other hand, the fingerprint-based approaches harness the naturally existing spatial features associated with different locations, e.g., RSSI, CIR, and CFR. In these schemes, fingerprints of different locations are stored in a database during the offline phase. In the online phase, the fingerprint of the current location is compared against those in the database to estimate the device location. In [13]–[15], RSSI values from multiple APs are utilized as the fingerprint, leading to an

Manuscript received June 23, 2016; revised October 8, 2016; accepted October 31, 2016. Date of publication November 15, 2016; date of current version February 8, 2017.

C. Chen and K. J. R. Liu are with Origin Wireless, Greenbelt, MD 20770 USA, and also with the Department of Electrical and Computer Engineering, University of Maryland at College Park, College Park, MD 20742 USA (e-mail: chen.chen@originwireless.net; ray.liu@originwireless.net).

Y. Chen was with Origin Wireless, Greenbelt, MD 20770 USA. He is now with the University of Electronic Science and Technology of China, Chengdu 611731, China (e-mail: eecyan@uestc.edu.cn).

Y. Han and H.-Q. Lai are with Origin Wireless, Greenbelt, MD 20770 USA (e-mail: yi.han@originwireless.net; quoc.lai@originwireless.net).

Digital Object Identifier 10.1109/JIOT.2016.2628701

accuracy of 2–5 m. Wu *et al.* [16] utilized multidimensional scaling to construct a stress-free floorplan as well as its associated fingerprint space containing the RSSI values obtained from locations on the stress-free floorplan for crowdsourcing-based indoor localization. The average error is around 2 m with the maximum error within 8 m. The accuracy can be further improved to 0.95–1.1 m by taking CFRs as the fingerprint [17]–[19]. Wu *et al.* [20] obtained CIR fingerprints under a bandwidth of 125 MHz and calculate the time-reversal (TR) resonating strength (TRRS) as the similarity measure among different locations, leading to an accuracy of 1–2 cm under NLOS scenarios.

Summarizing the ranging-based and fingerprint-based schemes, we find the following.

- 1) The accuracy of the ranging-based methods are susceptible to the correctness of the physical rules, e.g., path-loss model, which degrades severely in the complex indoor environment. The existence of a large number of multipath components and blockage of obstacles in indoor spaces impair the precision of the physical rules.
- 2) The fingerprint-based methods, which can work under strong NLOS environment, require a large bandwidth for accurate localization. Since the maximum bandwidth of the mainstream 802.11n is 40 MHz, IPSs utilizing WiFi techniques cannot resolve enough independent multipath components in the environment which introduces ambiguities into fingerprints associated with different locations. Thus, the localization performance is degraded. On the other hand, a bandwidth as large as 125 MHz that leads to centimeter accuracy [20] can only be achieved on dedicated hardware and incurs additional costs in deployment.

Is there any approach that can achieve the centimeter localization accuracy using WiFi devices in an NLOS environment? The answer is affirmative. Chen *et al.* [21] presented an IPS that achieves centimeter accuracy using one pair of single-antenna WiFi devices under strong NLOS conditions using frequency hopping. The IPS obtains CFRs and formulates location fingerprints from multiple WiFi channels in the offline phase, and calculates TRRS for localization in the online phase. However, interference from other WiFi networks might corrupt the fingerprint, which is neglected in [21]. To deal with the interference, in this paper, we introduce an additional step of CFR sifting. Moreover, we utilize CFR averaging to mitigate the impact of channel noise and refine the fingerprint. Additionally, we provide much more details and analysis on the experiment results. In comparison with most of the existing works that dedicate to mitigate the impact of multipath propagation, the proposed method embraces the multipath effect. Moreover, it is infrastructure-free since it is built upon the WiFi networks available in most indoor spaces.

The main contributions of this paper can be summarized as follows.

- 1) We propose an IPS that achieves centimeter accuracy in an NLOS environment with one pair of single-antenna WiFi devices. The proposed IPS eliminates the impact of interference from other WiFi networks through the process of CFR sifting.

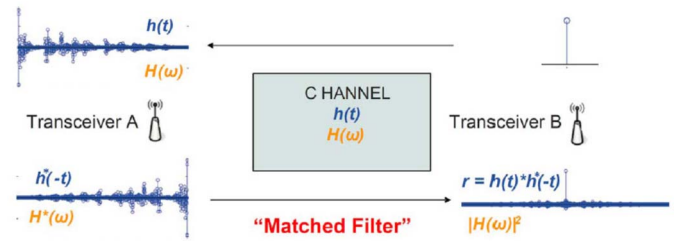


Fig. 1. Architecture of TR wireless communication system.

- 2) Leveraging the frequency diversity, we demonstrate that a large effective bandwidth can be achieved on WiFi devices by means of frequency hopping to overcome the issue of location ambiguity issue on traditional WiFi-based approaches.
  - 3) We conduct extensive experiments in a typical office environment to show the centimeter accuracy within an area of 20 cm  $\times$  70 cm under strong NLOS conditions.
- The rest of this paper is organized as follows. In Section II, we introduce the TR technique and the channel estimation in WiFi systems. In Section III, we elaborate on the proposed localization algorithm. In Section IV, we present the frequency hopping mechanism. In Section V, we demonstrate the experiment results in a typical office environment. In Section VI, we present some discussions on several aspects of the proposed IPS. Finally, we draw the conclusions in Section VII.

## II. PRELIMINARIES

In this part, we introduce the background of the TR technique and the channel estimation schemes in WiFi systems.

### A. Time-Reversal

TR is a signal processing technique capable of mitigating the phase distortion of a signal passing a linear time-invariant (LTI) filtering system. It is based upon the fact that when the LTI system  $h(t)$  is concatenated with its time-reversed and conjugated version  $h^*(-t)$ , the phase distortion is completely canceled out at a particular time instance.

A physical medium can be regarded as LTI if it satisfies inhomogeneity and invertibility. When both conditions hold, TR focuses the signal energy at a specific time and at a particular location, known as the spatial-temporal focusing effect. Such focusing effect is observed experimentally in the field of ultrasonics, acoustics, as well as electromagnetism [22]–[25]. Leveraging the focusing effect, TR is applied successfully to the broadband wireless communication systems [26].

Fig. 1 shows the architecture of the TR communication system consisting of two phases, namely, channel probing phase and transmission phase. Here, we assume that transceiver A intends to send some data to transceiver B. During the channel probing phase, transceiver B sends an impulse signal to transceiver A, and transceiver A extracts the CIR based on the impulse signal, time-reverses, and takes conjugate of the CIR to generate a waveform. During the transmission phase, transceiver A convolves the transmitted signal with the waveform and sends to transceiver B. In this process, the channel

acts as a natural matched filter due to the TR operation. The TR focusing effect could be observed at a specific time instance and only at the exact location of transceiver  $B$ .

In virtue of the high-resolution TR focusing effect, in this paper, we utilize TR as the signal processing technique to measure the similarity among fingerprints of different locations.

### B. Channel Estimation in WiFi Systems

In a WiFi system adopting the orthogonal frequency-division multiplexing (OFDM) scheme, the transmitted data symbols are spread onto multiple subcarriers to combat against the frequency-selective fading incurred by the multipath effect. Assuming a total of  $K$  usable subcarriers and denote the transmitted frequency domain data symbol on the  $k$ th subcarrier with index  $u_k$  as  $X_{u_k}$ , the received frequency domain signal on subcarrier  $u_k$ , denoted by  $Y_{u_k}$ , takes the form as [27]

$$Y_{u_k} = H_{u_k}X_{u_k} + W_{u_k}, \quad k = 1, 2, \dots, K \quad (1)$$

where  $H_{u_k}$  is the CFR on subcarrier  $u_k$  and  $W_{u_k}$  is the complex Gaussian noise on subcarrier  $u_k$ . The estimation of  $H_{u_k}$  in the least-square sense takes the form

$$\hat{H}_{u_k} = \frac{Y_{u_k}}{X_{u_k}} = H_{u_k} + W'_{u_k}, \quad k = 1, 2, \dots, K \quad (2)$$

where  $W'_{u_k} = (W_{u_k}/X_{u_k})$  given *a priori* knowledge of  $X_{u_k}$ .

Equation (2) is only valid in the absence of synchronization errors, which cannot be neglected in practice. The synchronization errors mainly consist of: 1) channel frequency offset (CFO); 2) sampling frequency offset (SFO); and 3) symbol timing offset (STO). The CFO, denoted as  $\Delta f$ , is caused by the misalignment of the local oscillators at the transmitter and receiver. Given  $N$  samples per OFDM block and a sampling interval of  $T_s$ , the normalized CFO  $\epsilon$  can be written as  $\Delta f N T_s$ . The SFO, denoted as  $\eta$ , is introduced by the mismatch between the sampling interval at the transmitter and that at the receiver. Given a sampling interval of  $T_s$  at the transmitter side and a sampling interval of  $T'_s$  at the receiver side,  $\eta$  can be expressed as  $(T'_s - T_s)/T_s$ . The STO, denoted as  $\Delta n_0$ , is caused by the imperfect timing synchronization at the receiver. These synchronization errors introduce additional phase rotations as well as amplitude attenuation into  $\hat{H}_{u_k}$ . Although the WiFi receivers perform timing and frequency synchronizations, the residual of these errors cannot be neglected.

Denote the estimated CFR associated with the  $i$ th received OFDM symbol on the  $k$ th subcarrier as  $\hat{H}_i^{u_k}$ . In the presence of the residual synchronization errors,  $\hat{H}_i^{u_k}$  can be modified from (2) into [28]

$$\hat{H}_i^{u_k} = \text{sinc}(\pi(\Delta\epsilon + \Delta\eta u_k))H_{u_k}e^{j2\pi(\beta_i u_k + \alpha_i)} + W'_{i,u_k} \quad (3)$$

for  $k = 1, 2, \dots, K$ , where

$$\alpha_i = \left( \frac{1}{2} + \frac{iN_s + N_g}{N} \right) \Delta\epsilon \quad (4)$$

$$\beta_i = \frac{\Delta n_0}{N} + \left( \frac{1}{2} + \frac{iN_s + N_g}{N} \right) \Delta\eta \quad (5)$$

are the initial and linear phase distortions, respectively. Here,  $\Delta\epsilon$  and  $\Delta\eta$  represent the residual errors of the normalized

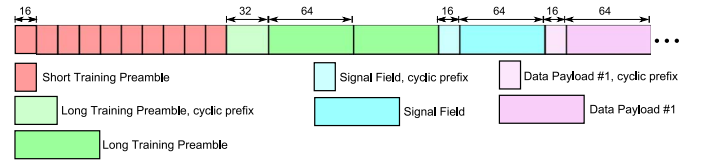


Fig. 2. Frame structure for 802.11a.

CFO  $\epsilon$  and the normalized SFO  $\eta$ , respectively.  $\text{sinc}(\pi(\Delta\epsilon + \Delta\eta u_k))$  is the amplitude attenuation and can be approximated as 1 given typical values of  $\Delta\epsilon$  and  $\Delta\eta$ .  $N_g$  is the length of the cyclic prefix,  $N_s$  is the total length of one OFDM frame with length  $N + N_g$ , and  $W'_{i,u_k}$  is the estimation noise on subcarrier  $u_k$  for the  $i$ th OFDM symbol that can be modeled as complex Gaussian noise [29].

In practice, preambles are utilized at the WiFi receiver to assist synchronization and channel estimation. Fig. 2 demonstrates the physical layer (PHY) frame structure of 802.11a [30]. Before the transmission of the data payloads, the WiFi transmitter sends preambles composed by short training preambles (STPs), long training preambles (LTPs), and cyclic prefix. The WiFi receiver performs timing and frequency synchronization using the STPs and then compensates the synchronization errors. Since the receiver has the full knowledge of the OFDM symbols of the LTPs, it performs channel estimation based on the LTPs to extract the CFRs, which leads to  $\hat{H}_i^{u_k}$  as shown in (3).

## III. PROPOSED ALGORITHM

### A. Calculation of TRRS in Frequency Domain

In the proposed IPS, the similarity between two locations is measured by the TRRS between their fingerprints. In this section, we provide details of TRRS computation.

Given two time-domain CIRs  $\hat{\mathbf{h}}$  and  $\hat{\mathbf{h}}'$ , with  $\hat{\mathbf{h}} = [\hat{h}[0], \hat{h}[1], \dots, \hat{h}[L-1]]^T$  and  $\hat{\mathbf{h}}'$  defined similarly, where  $T$  is the transpose operator, the TRRS between  $\hat{\mathbf{h}}$  and  $\hat{\mathbf{h}}'$  is calculated as [20]

$$\gamma_{\text{CIR}}[\hat{\mathbf{h}}, \hat{\mathbf{h}}'] = \frac{\max_i |(\hat{\mathbf{h}} * \hat{\mathbf{g}})[i]|^2}{\langle \hat{\mathbf{h}}, \hat{\mathbf{h}} \rangle \langle \hat{\mathbf{g}}, \hat{\mathbf{g}} \rangle} \quad (6)$$

where  $*$  denotes the convolution operator,  $\hat{\mathbf{g}}$  is the time-reversed and conjugate version of  $\hat{\mathbf{h}}'$ , and  $\langle \mathbf{x}, \mathbf{y} \rangle$  is the inner product operator between complex vector  $\mathbf{x}$  and complex vector  $\mathbf{y}$ , expressed by  $\mathbf{x}^\dagger \mathbf{y}$  where  $(\cdot)^\dagger$  is the Hermitian operator. Notice that, the computation of  $\gamma_{\text{CIR}}[\hat{\mathbf{h}}, \hat{\mathbf{h}}']$  removes the impact of STO by searching all possible index  $i$  across the output of  $|(\hat{\mathbf{h}} * \hat{\mathbf{g}})[i]|$ . It can be shown that  $0 \leq \gamma_{\text{CIR}}[\hat{\mathbf{h}}, \hat{\mathbf{h}}'] \leq 1$ .

Since the convolution in the time domain can be cast to the inner product in the frequency domain [31], the TRRS can be calculated using CFRs, the frequency-domain counterparts of CIRs. Given two CFRs  $\hat{\mathbf{H}} = [\hat{H}_{u_1}, \hat{H}_{u_2}, \dots, \hat{H}_{u_K}]^T$  and  $\hat{\mathbf{H}}'$  defined similarly, and assume that the synchronization

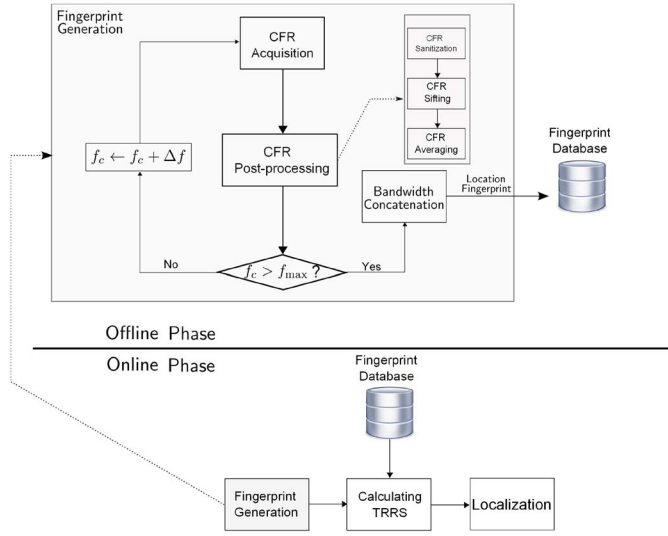


Fig. 3. Flowchart of the algorithm.

errors are mostly mitigated, the TRRS in frequency domain is given by

$$\gamma[\hat{\mathbf{H}}, \hat{\mathbf{H}}'] = \frac{\left| \sum_{k=1}^K \hat{H}_{uk} \hat{H}'_{uk} \right|^2}{\langle \hat{\mathbf{H}}, \hat{\mathbf{H}} \rangle \langle \hat{\mathbf{H}}', \hat{\mathbf{H}}' \rangle}. \quad (7)$$

It is straightforward to prove that  $0 \leq \gamma[\hat{\mathbf{H}}, \hat{\mathbf{H}}'] \leq 1$ , and  $\gamma[\hat{\mathbf{H}}, \hat{\mathbf{H}}'] = 1$  if and only if  $\hat{\mathbf{H}} = C\hat{\mathbf{H}}'$  where  $C \neq 0$  is any complex scaling factor. Therefore, the TRRS can be regarded as a measure of similarity between two CFRs.

### B. Indoor Localization Based on TRRS

The proposed localization algorithm consists of an offline phase and an online phase. The details of the two phases are illustrated in Fig. 3 and are elaborated below.

1) *Offline Phase:* In the offline phase, the CFRs are measured at  $D$  channels, denoted by  $f_1, f_2, \dots, f_d, \dots, f_D$ , and at  $L$  locations-of-interest, denoted by  $1, 2, \dots, l, \dots, L$ . Assume that a total of  $N_{\ell, f_d}$  CFRs are measured from the first and second LTPs at location  $\ell$  and channel  $f_d$ , we write the CFR matrix as

$$\hat{\mathbb{H}}_i[\ell, f_d] = \left[ \hat{\mathbf{H}}_{i,1}[\ell, f_d] \cdots \hat{\mathbf{H}}_{i,m}[\ell, f_d] \cdots \hat{\mathbf{H}}_{i, N_{\ell, f_d}}[\ell, f_d] \right] \quad (8)$$

where  $m = 1, 2, \dots, N_{\ell, f_d}$  is the realization index,  $i \in \{1, 2\}$  is the LTP index, and  $\hat{\mathbf{H}}_{i,m}[\ell, f_d] = [\hat{H}_{i,m}^{u_1}[\ell, f_d] \cdots \hat{H}_{i,m}^{u_k}[\ell, f_d] \cdots \hat{H}_{i,m}^{u_K}[\ell, f_d]]^T$  with  $\hat{H}_{i,m}^{u_1}[\ell, f_d]$  standing for the  $m$ th CFR of the  $i$ th LTP on subcarrier  $u_k$ , and at location  $\ell$ , channel  $f_d$ .

The location fingerprint is generated from  $\hat{\mathbb{H}}_i[\ell, f_d]$ . The process contains four steps, which are presented below.

a) *CFR sanitization:* The captured CFRs must be sanitized so as to mitigate the impact of initial and linear phase distortions shown in (3). First of all, we estimate the residual CFO and SFO from the channel estimation using [32]

$$\begin{aligned} \Omega_m^{u_k}[\ell, f_d] &= \left[ \hat{H}_{1,m}^{u_k}[\ell, f_d] \right]^* \times \hat{H}_{2,m}^{u_k}[\ell, f_d] \\ &= e^{j2\pi \frac{N_s}{N} \phi_{u_k}} |H_{1,m}^{u_k}[\ell, f_d]|^2 + \psi_m^{u_k}[\ell, f_d] \end{aligned} \quad (9)$$

where  $\phi_k = \Delta\epsilon + \Delta\eta k$  and  $\psi_m^{u_k}[\ell, f_d]$  contains all cross terms. Therefore,  $\phi_{u_k}$  can be estimated by

$$\hat{\phi}_{u_k} = \angle[\Omega_m^{u_k}[\ell, f_d]] \quad (10)$$

where  $\angle[X]$  is the angle of  $X$  measured in radians. Compensating for  $\hat{\phi}_{u_k}$  gives

$$\tilde{H}_{i,m}^{u_k}[\ell, f_d] = \hat{H}_{i,m}^{u_k}[\ell, f_d] e^{-j\pi \hat{\phi}_{u_k}} e^{-j2\pi \frac{N_g + (i-1)N_s}{N} \hat{\phi}_{u_k}}. \quad (11)$$

Substituting (11) into (8) and writing the updated  $\hat{\mathbb{H}}_i[\ell, f_d]$  in (8) as  $\tilde{\mathbb{H}}_i[\ell, f_d]$ , we take the average of  $\tilde{\mathbb{H}}_1[\ell, f_d]$  and  $\tilde{\mathbb{H}}_2[\ell, f_d]$  as  $\tilde{\mathbb{H}}[\ell, f_d] = (\tilde{\mathbb{H}}_1[\ell, f_d] + \tilde{\mathbb{H}}_2[\ell, f_d])/2$ .

After the removal of residual CFO and SFO, the STO still remains to be compensated. Write

$$\tilde{\mathbb{H}}[\ell, f_d] = \left[ \tilde{\mathbf{H}}_1[\ell, f_d] \cdots \tilde{\mathbf{H}}_m[\ell, f_d] \cdots \tilde{\mathbf{H}}_{N_{\ell, f_d}}[\ell, f_d] \right] \quad (12)$$

where  $\tilde{\mathbf{H}}_m[\ell, f_d] = [\tilde{H}_m^{u_1}[\ell, f_d] \cdots \tilde{H}_m^{u_k}[\ell, f_d] \cdots \tilde{H}_m^{u_K}[\ell, f_d]]^T$  is the CFR vector for the  $m$ th realization on usable subcarriers after CFO/SFO correction. Denoting  $A_m^{u_k}[\ell, f_d] = \angle\{\tilde{H}_m^{u_k}[\ell, f_d]\}$  as the angle of  $\tilde{H}_m^{u_k}[\ell, f_d]$ , we perform phase unwrapping on  $A_m^{u_k}[\ell, f_d]$  to yield  $A_m'^{u_k}[\ell, f_d]$ . The slope of  $A_m'^{u_k}[\ell, f_d]$  is linear with STO if we disregard the noise and interference. To estimate the slope, we perform a least-square fitting on  $A_m'^{u_k}[\ell, f_d]$  expressed by

$$\widehat{\Delta n_0} = \frac{N \sum_{k=1}^K [(u_k - \bar{u})] [A_m'^{u_k}[\ell, f_d] - \bar{A}]}{2\pi \sum_{k=1}^K [u_k - \bar{u}]^2} \quad (13)$$

where  $\bar{u} = (\sum_{k=1}^K u_k / K)$  and  $\bar{A} = (\sum_{k=1}^K A_m'^{u_k}[\ell, f_d] / K)$ . Therefore,  $\tilde{H}_m^{u_k}[\ell, f_d]$  is compensated as

$$\check{H}_m^{u_k}[\ell, f_d] = \tilde{H}_m^{u_k}[\ell, f_d] e^{-ju_k \text{round}(\widehat{\Delta n_0}) \frac{2\pi}{N}} \quad (14)$$

where  $\text{round}(x)$  rounds the argument  $x$  to its nearest integer. The compensated CFR matrix is denoted by

$$\check{\mathbb{H}}[\ell, f_d] = \left[ \check{\mathbf{H}}_1[\ell, f_d] \cdots \check{\mathbf{H}}_m[\ell, f_d] \cdots \check{\mathbf{H}}_{N_{\ell, f_d}}[\ell, f_d] \right]. \quad (15)$$

b) *CFR sifting:* Due to the presence of other WiFi devices in the environment, some CFR measurements might suffer from interference from nearby WiFi devices or other radio-frequency systems such as bluetooth, and should be excluded from further calculations. The interference introduces random noise onto the CFRs and impairs the CFR qualities. To combat the interference, first, we use  $\check{\mathbf{H}}_m[\ell, f_d]$  to calculate the  $N_{\ell, f_d} \times N_{\ell, f_d}$  TRRS matrix  $\mathbb{R}_{\ell, f_d}$ , where  $\check{\mathbf{H}}_m[\ell, f_d] = [\check{H}_m^{u_1}[\ell, f_d] \cdots \check{H}_m^{u_k}[\ell, f_d] \cdots \check{H}_m^{u_K}[\ell, f_d]]^T$  with  $\gamma[\cdot, \cdot]$  defined in (7). The  $(i, j)$ th entry of  $\mathbb{R}_{\ell, f_d}$  is

$$[\mathbb{R}_{\ell, f_d}]_{i,j} = \gamma[\check{\mathbf{H}}_i[\ell, f_d], \check{\mathbf{H}}_j[\ell, f_d]]. \quad (16)$$

Second, we compute the column-wise average of  $\mathbb{R}_{\ell, f_d}$  denoted as  $O_j$  with  $j = 1, 2, \dots, N_{\ell, f_d}$ , given by

$$O_j = \frac{1}{N_{\ell, f_d} - 1} \sum_{\substack{i=1, 2, \dots, N_{\ell, f_d} \\ i \neq j}} [\mathbb{R}_{\ell, f_d}]_{i,j}. \quad (17)$$

Finally, we remove the  $j$ 'th column of  $\check{\mathbb{H}}[\ell, f_d]$  if  $O_j \leq \tau$ , where  $\tau$  is a threshold.

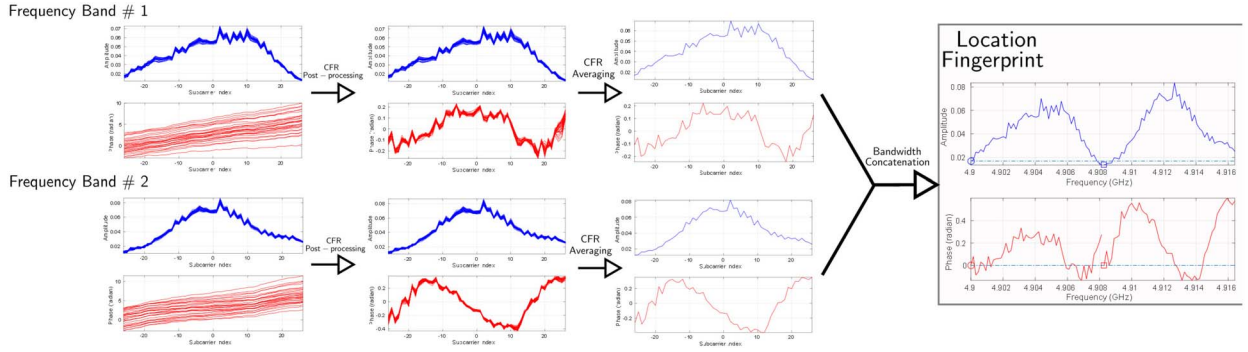


Fig. 4. Example of CFR post-processing, channel fingerprint generation, and location fingerprint generation.

We assume that the number of remaining CFRs after CFR sifting is  $N'_{\ell,fd}$ , and the corresponding index of the remaining CFRs are  $t_1, \dots, t_m, \dots, t_{N'_{\ell,fd}}$ .

c) *CFR averaging*: At location  $\ell$ , for channel  $f_d$ , we generate the averaged CFR  $\mathbf{S}[\ell, f_d] = [S_{\ell,fd}^{u_1} \dots S_{\ell,fd}^{u_k} \dots S_{\ell,fd}^{u_K}]^T$  with dimension  $K \times 1$  as

$$\mathbf{S}[\ell, f_d] = \frac{1}{N'_{\ell,fd}} \sum_{m=1}^{N'_{\ell,fd}} \check{\mathbf{H}}_{t_m}[\ell, f_d] \cdot \mathbf{W}_m \quad (18)$$

where  $\cdot$  stands for the element-wise dot product between two vectors.  $\mathbf{W}_m$  is a  $K \times 1$  vector represented as

$$\mathbf{W}_m = [w_m[\ell, f_d] \quad w_m[\ell, f_d] \quad \dots \quad w_m[\ell, f_d]]^T \quad (19)$$

where  $w_m[\ell, f_d] = e^{j(\angle[\check{H}_{t_1}^{u_1}[\ell, f_d]] - \angle[\check{H}_{t_m}^{u_1}[\ell, f_d]])}$ . The purpose of introducing  $\mathbf{W}_m$  is to match the initial phases of  $\check{\mathbf{H}}_{t_m}[\ell, f_d]$  with  $m > 1$  to the first realization  $\check{\mathbf{H}}_{t_1}[\ell, f_d]$ , so that  $\check{\mathbf{H}}_{t_m}[\ell, f_d]$  can be accumulated coherently, and the noise variance contained in  $\check{\mathbf{H}}_{t_m}[\ell, f_d]$  is reduced by  $N'_{\ell,fd}$  times consequently.

d) *Bandwidth concatenation*: At location  $\ell$ , we obtain the fingerprint vector with dimension  $DK \times 1$  by concatenating the averaged CFRs from all channels  $\{f_d\}_{d=1,2,\dots,D}$  as

$$\mathbf{G}[\ell] = [\mathbf{S}^T[\ell, f_1]V_1 \dots \mathbf{S}^T[\ell, f_d]V_d \dots \mathbf{S}^T[\ell, f_D]V_D]^T \quad (20)$$

where  $V_d = e^{-j\angle[S_{\ell,fd}^{u_1}]}$  is introduced to nullify the initial phases of different  $\mathbf{S}^T[\ell, f_d]$ .

Fig. 4 demonstrates an example of the fingerprint generation procedure. As can be observed from Fig. 4, the CFR post-processing effectively removes the phase distortions caused by the synchronization errors. The CFR averaging combines different realizations coherently, and the bandwidth concatenation associates the two averaged CFR into the location fingerprint.

Since we concatenate all available bandwidths from  $D$  channels, we achieve a much larger effective bandwidth denoted by  $W_e = DW$ , where  $W$  is the bandwidth per channel.

2) *Online Phase*: The CFRs from an unknown location are formulated into the location fingerprint in the same manner as described in the offline phase. Assume that the location fingerprint from the unknown location  $\ell'$  is given by  $\mathbf{G}[\ell']$ , the TRRS between location  $\ell'$  and location  $\ell$  is computed as  $\gamma[\mathbf{G}[\ell], \mathbf{G}[\ell']]$ . Define  $\ell^* = \underset{\ell=1,2,\dots,L}{\operatorname{argmax}} \gamma[\mathbf{G}[\ell], \mathbf{G}[\ell']]$ , the

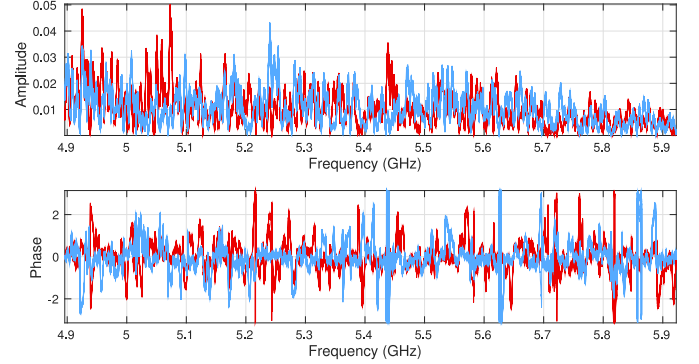


Fig. 5. Snapshot of location fingerprints after bandwidth concatenation at two different locations.

estimated location  $\hat{\ell}'$  takes the form

$$\hat{\ell}' = \begin{cases} \ell^*, & \text{if } \gamma[\mathbf{G}[\ell^*], \mathbf{G}[\ell']] \geq \Gamma \\ 0, & \text{Otherwise} \end{cases} \quad (21)$$

where  $\Gamma$  is a tunable threshold. Notice that, in case of  $\gamma[\mathbf{G}[\ell^*], \mathbf{G}[\ell']] < \Gamma$ , the proposed IPS fails to localize the device, and the algorithm returns 0 to imply an *unknown location*.

In Fig. 5, we show an example of location fingerprints generated at two different locations in different colors. For each location, we formulate 5 location fingerprints. As we can see, the differences among the location fingerprints at the same location are minor, while the differences of location fingerprints between the two different locations are much more pronounced.

#### IV. FREQUENCY HOPPING MECHANISM

In this section, we elaborate on the implementation details of the proposed IPS.

##### A. CFR Acquisition Using USRPs

We build two Universal Software Radio Peripherals (USRPs) N210 [33] into prototypes for localization. Each USRP is equipped with one omnidirectional antenna.

Bloessl *et al.* [34] developed a WiFi transceiver supporting WiFi standards 802.11a/g/p under the framework of GNU Radio [35]. The proposed WiFi transceiver in [34] extracts the

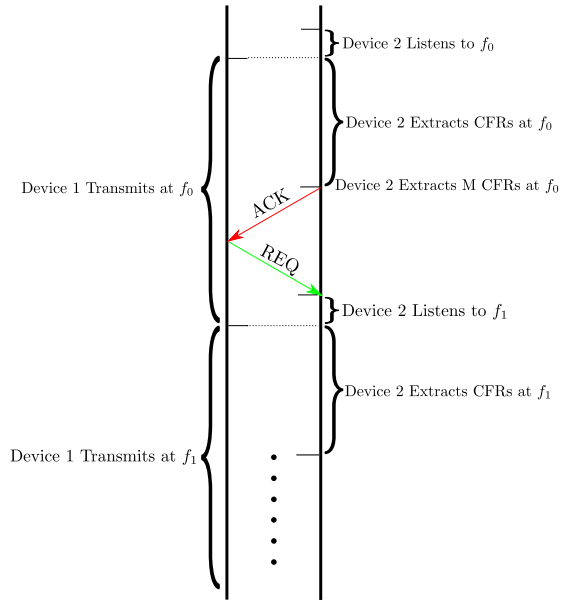


Fig. 6. Timing diagram of the frequency hopping mechanism.

CFRs by the 4 frequency-domain subcarrier pilots followed by an interpolation to fully recover the CFRs on the 48 usable data subcarriers. However, due to the scarcity of the subcarrier pilots, the estimated CFRs are not accurate enough to provide fine details about the environment to facilitate indoor localization.

To acquire CFRs with high quality, we extend the framework in [34] by including a channel estimator leveraging the two LTPs as shown in the WiFi frame structure in Fig. 2. Each LTP is composed by 56 data subcarriers which are known in advance at the receiver side, and the CFRs are extracted using (2) in Section II. To reduce the impact of synchronization errors on the CFRs, we estimate and compensate the STO, SFO, and CFO using the STPs as shown in Fig. 2. The estimated and compensated CFRs are used to equalize the signal field frame which contains the information of the coding rate as well as the signal constellation of the transmitted OFDM symbols. Then, the receiver decodes the data payloads based on this information.

We also notice that the framework in [34] lacks the mechanism of carrier sense multiple access. Therefore, interference from other WiFi devices cannot be avoided. In light of this issue, we only keep those CFRs associated with the data payloads which could be successfully decoded.

### B. Implementing the Frequency Hopping Mechanism

In the proposed IPS, frequency hopping is used to acquire CFRs from a multitude of frequency bands. In Fig. 6, we demonstrate the timing diagram of the mechanism of synchronous frequency hopping with feedback between two devices from the center frequency  $f_0$  to  $f_1$ . Here, ACK stands for the acknowledgment frame, and REQ denotes the frequency hopping request frame. Device 2 initializes the procedure by tuning its center frequency at  $f_0$ . Then, device 1 starts transmission at  $f_0$  as well to facilitate CFR acquisition

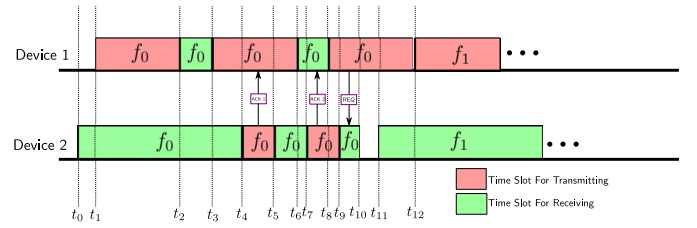


Fig. 7. Timing diagram for frequency hopping.

on device 2. Assume that the minimum number of CFRs per frequency band is  $M_{\min}$ . After obtaining  $M_{\min}$  CFRs at  $f_0$ , device 2 sends an ACK frame to device 1, and device 1 feeds back an REQ frame to device 2. On reception of the REQ frame, device 2 adjusts its center frequency to  $f_1$ , and device 1 begins transmission at  $f_1$ .

In Fig. 6, we assume that the two devices perform full-duplex communication, i.e., transmitting signals while listening simultaneously to acquire the ACK and REQ frames. However, in practice, the USRP N210 devices in the proposed IPS are half-duplex, i.e., one device cannot perform WiFi transmitting and receiving at the same time. Thus, each device needs to switch between the transmitting mode and the receiving mode in different time slots. Fig. 7 shows an example of frequency hopping from  $f_0$  to  $f_1$ . The details for each time-of-interest denoted as  $t_1, t_2, \dots, t_{12}$  in Fig. 7 are presented below.

- $t_0$ : Device 2 (D2) tunes its center frequency to  $f_0$  and stays in the receiving mode.
- $t_1$ : Device 1 (D1) tunes its center frequency to  $f_0$  and begins data transmission. D2 detects the presence of data transmission and performs channel estimation to extract CFRs from each data frame. Device D2 stays in the receiving mode until the number of CFRs exceeds  $M_{\min}$ .
- $t_2$ : D1 switches to receiving mode to determine whether D2 sends an acknowledgment signal (ACK) by encoding the message in the data payloads. Suppose that at this moment, D2 obtains  $M' < M_{\min}$  CFRs. Since the number of CFRs is insufficient, D2 still stays in the receiver mode. Notice that, if D2 acquires sufficient CFRs in this stage, D2 would switch to the transmitter mode and send an ACK frame to D1, and the procedure would continue from  $t_7$ .
- $t_3$ : D1 does not receive the ACK frame from D2 and thus switches back to the transmitter mode and continues data transmission.
- $t_4$ : D2 receives the targeted  $M_{\min}$  CFRs and switches to the transmitter mode. It then transmits an ACK signal to D1. Nevertheless, since D1 is in transmitter mode, the ACK signal transmission fails.
- $t_5$ : D2 switches to receiver mode to decide whether D1 sends a frequency hopping request (REQ) which is encoded into the data payloads. Due to the failure of the ACK signal transmission at  $t_4$ , D1 is unable to send the REQ signal.
- $t_6$ : D1 switches to the receiver mode again.

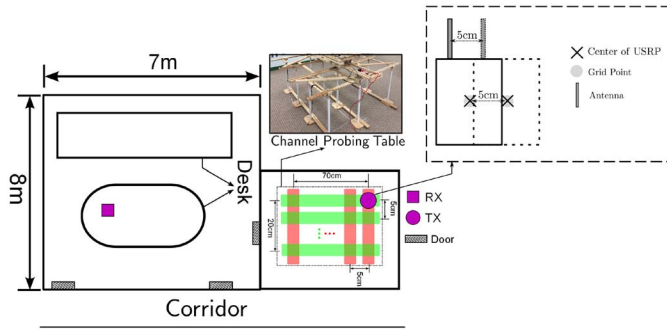


Fig. 8. Experiment settings.

- $t_7$ : D2 switches to the transmitter mode again and sends out another ACK signal.
- $t_8$ : D1 receives the ACK signal and switches to the transmitter mode to send out an REQ. However, Device 2 is still in the transmitter mode and cannot receive the request at this moment.
- $t_9$ : D2 switches to the receiver mode and receives the REQ signal because that D1 stays in the transmitter mode.
- $t_{10}$ : D2 begins the process of tuning its center frequency to  $f_1$ .
- $t_{11}$ : D2 successfully tunes its center frequency to  $f_1$  and awaits the transmission from D1 at  $f_1$  as well. Since D1 is still transmitting using  $f_0$ , D2 is unable to decode the signal.
- $t_{12}$ : D1 also tunes its center frequency to  $f_1$  and begins transmission.

The same protocol is repeated until CFRs from all desirable frequency bands are measured.

## V. EXPERIMENT RESULTS

### A. Experiment Settings

Fig. 8 shows the setups of the experiments with details given below.

1) *Environment*: The experiments are conducted in a typical office suite composed by a large and a small office room in a multistorey building. The two office rooms are blocked by a wall. In addition to the two large desks, the indoor space is filled with other furniture including chairs and computers, which are not shown in Fig. 8 for brevity.

2) *Configurations*: Two USRPs are used to obtain the CFRs with bandwidth configured as  $W = 10$  MHz. The two USRPs coordinate with each other to perform synchronous frequency hopping using the mechanism discussed in Section IV. The step size of frequency hopping is fixed at  $\Delta f = 8.28$  MHz.<sup>1</sup> The minimum number of CFRs per channel is set as  $M_{\min} = 10$ .

3) *Details of Measurement*: One USRP is placed on the grid points on a measurement platform in the small room as shown in Fig. 8. The center of the USRP is aligned with the

<sup>1</sup>Considering the null subcarriers at both edges of the WiFi channel spectrum, we adjust the frequency hopping step size such that the entire spectrum can be covered without spectrum holes. Notice that the proposed IPS does not require the measured frequency band to be contiguous.

grid point. The distance between two adjacent grid points is 5 cm. The other USRP is placed on the table of the larger room. CFRs from  $L = 75$  different grid points are measured within an area of  $70 \text{ cm} \times 20 \text{ cm}$ . For each measurement, the two USRPs sweep the frequency band from 4.9 to 5.9 GHz, leading to a total of  $D = 124$  times of frequency hopping with a step size of 8.28 MHz. The effective bandwidth  $W_e$  is thus 1 GHz. For each of the 75 locations, we formulate  $M = 10$  location fingerprints.

### B. Metrics for Performance Evaluation

For the  $M = 10$  fingerprints collected at each location, we store the first  $M_1 = 5$  CFRs into the fingerprint database in the offline phase, and consider the other  $M_2 = 5$  fingerprints as samples collected in the online phase. Denote the  $m$ th location fingerprint formulated at location  $\ell$  as  $\mathbf{G}_m[\ell]$ , we calculate the TRRS matrix  $\mathbb{R}$  with the  $(i, j)$ th entry of  $\mathbb{R}$  given by  $\gamma[\mathbf{G}_m[\ell], \mathbf{G}_n[\ell']]$ , where  $m = \text{Mod}(i, M_1) + 1$ ,  $\ell = [(i - m - 1)/M_1] + 1$ ,  $n = \text{Mod}(j, M_2) + 1$ , and  $\ell' = [(j - n - 1)/M_2] + 1$ . Here,  $\text{Mod}$  is the modulus operator,  $i$  is termed as the training index, and  $j$  is termed as the testing index.

We define the entries of  $\mathbb{R}$  calculated from CFRs obtained at the same locations as the *diagonal entries*, while those calculated using CFRs obtained from different locations as the *off-diagonal entries*. We demonstrate the histograms and cumulative density functions for the diagonal and off-diagonal entries.

Based on  $\mathbb{R}$ , we evaluate the localization performances using the metrics of the true positive rate, denoted as  $P_{\text{TP}}$ , and the false positive rate, denoted as  $P_{\text{FP}}$ .  $P_{\text{TP}}$  is defined as the probability that the IPS localizes the device to its correct location, while  $P_{\text{FP}}$  captures the probability that the IPS localizes the device to a wrong location, or fails to localize the device.

In the performance evaluation, the CFR sifting parameter  $\tau$  is set as 0.8.

### C. Performance Evaluation

1) *TRRS Matrix Under Different  $W_e$* : Fig. 9 demonstrates  $\mathbb{R}$  with  $W_e \in [10, 40, 120, 1000]$  MHz. We observe that when  $W_e = 10$  MHz, there exists many large off-diagonal entries in  $\mathbb{R}$ , indicating severe ambiguities among different locations. When the total bandwidth  $W_e$  increases, the ambiguities among different locations are significantly eliminated, while the TRRS within the same location are almost unchanged.

2) *Distribution of Diagonal and Off-Diagonal Entries Under Different  $W_e$* : Fig. 10 visualizes the distribution of the diagonal and off-diagonal entries of  $\mathbb{R}$  with different  $W_e \in [10, 40, 120, 1000]$  MHz using histograms. Statistics of the diagonal and off-diagonal entries are shown as well. As we can see, the TRRS values at the same locations are identical with different  $W_e$ , implying high stationarity of the proposed IPS. On the other hand, the off-diagonal entries are more suppressed and approach a Gaussian-like distribution when  $W_e$  increases. We also observe an enlarged

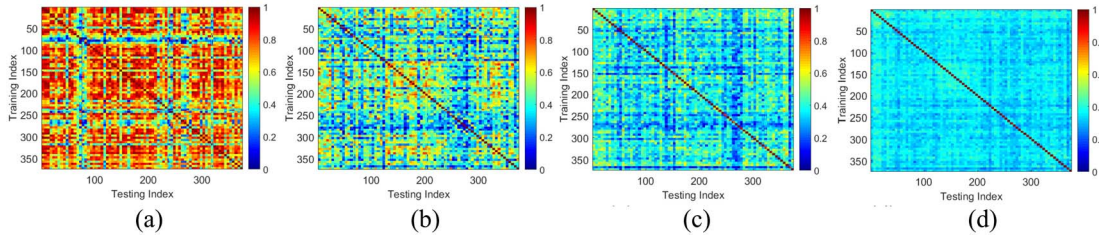


Fig. 9. TRRS matrix under different  $W_e$ . (a)  $W_e = 10$  MHz. (b)  $W_e = 40$  MHz. (c)  $W_e = 120$  MHz. (d)  $W_e = 1000$  MHz.

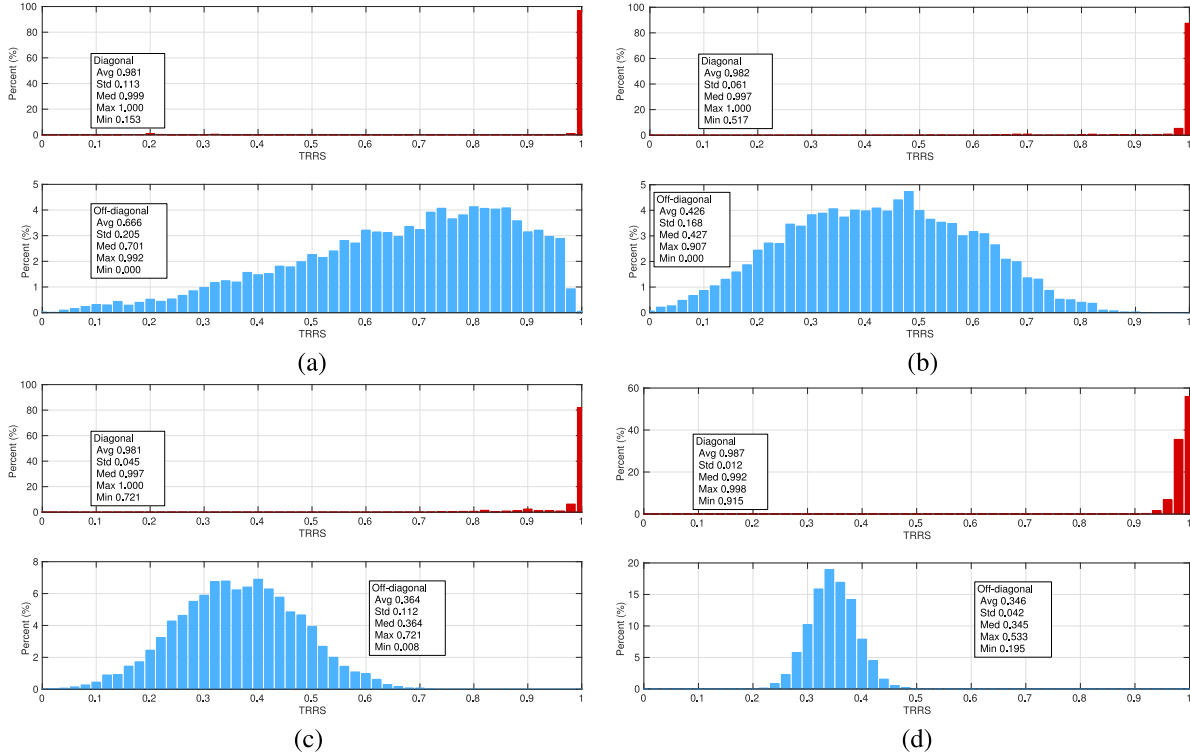


Fig. 10. Histogram of diagonal and off-diagonal entries under different  $W_e$ . (a)  $W_e = 10$  MHz. (b)  $W_e = 40$  MHz. (c)  $W_e = 120$  MHz. (d)  $W_e = 1000$  MHz.

gap between the diagonal and off-diagonal entries when  $W_e$  increases, indicating a better separability among different locations. The increase of  $W_e$  also reduces the variations of diagonal and off-diagonal entries, as shown by the decreasing standard deviations. Moreover, a large  $W_e$  removes the outliers in the diagonal entries: when  $W_e = 10$  MHz, the minimum value of diagonal entries is 0.153, while the minimum value increases to 0.915 when  $W_e = 1000$  MHz. Thus, a large  $W_e$  improves the robustness of the IPS against outliers.

### 3) Cumulative Density Functions of Diagonal and Off-Diagonal Entries Under Different $W_e$ :

In Fig. 11, we demonstrate the cumulative density functions of diagonal and off-diagonal entries with  $W_e \in [10, 20, 40, 80, 120, 300, 500, 1000]$  MHz. As can be seen from the figure, a large  $W_e$  reduces the spread of both the diagonal and off-diagonal entries, which agrees with the results shown in Fig. 10.

### 4) Mean and Standard Deviation Performances Under Different $W_e$ :

Fig. 12 depicts the impact of  $W_e$  on the mean and standard deviation performances for both diagonal and

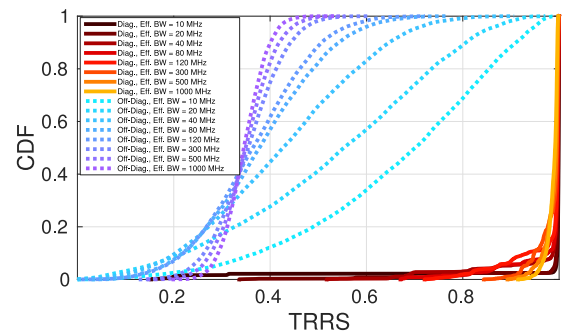


Fig. 11. Cumulative density functions of diagonal and off-diagonal entries of the TRRS matrix under different  $W_e$ .

off-diagonal entries. The upper and lower bars indicate the  $\pm\sigma$  bounds with respect to the average, where  $\sigma$  stands for the standard deviation. We conclude that: a large  $W_e$  improves the distinction among different locations, but also reduces the variation of the TRRS at the same locations as well as among different locations. In other words, a large  $W_e$  makes the IPS performance more stable and predictable.

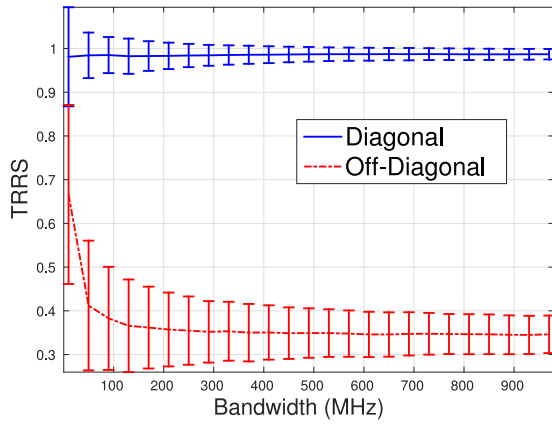


Fig. 12. Mean and standard deviation of the diagonal and off-diagonal entries of the TRRS matrix under different  $W_e$ .

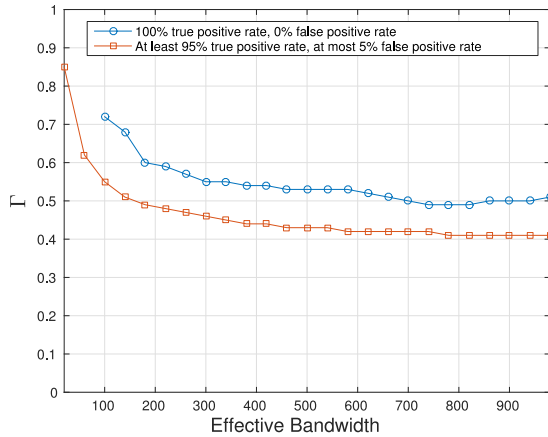


Fig. 13. Threshold  $\Gamma$  under different  $W_e$  to achieve: 1)  $P_{TP} = 100\%$  and  $P_{FP} = 0\%$  and 2)  $P_{TP} \geq 95\%$  and  $P_{FP} \leq 5\%$ .

5) *Threshold  $\Gamma$  Settings Under Different  $W_e$ :* Fig. 13 depicts the smallest threshold  $\Gamma$  under  $W_e = [20, 60, 100, \dots, 1000]$  MHz to achieve: 1)  $P_{TP} = 100\%$  and  $P_{FP} = 0\%$  and 2)  $P_{TP} \geq 95\%$  and  $P_{FP} \leq 5\%$ . We observe a decreasing in  $\Gamma$  when  $W_e$  is larger, which can be justified by the fact that the gap between the diagonal and off-diagonal entries enlarges when  $W_e$  becomes larger. When  $W_e = 20$  MHz, the IPS fails to achieve  $P_{TP} = 100\%$  and  $P_{FP} = 0\%$ . Fig. 13 also implies that we can achieve a perfect 5 cm localization if  $\Gamma$  is chosen appropriately.

Based on the experiment results, we conclude that a large  $W_e$  is imperative for the robustness, stability, and performance of the proposed IPS. By formulating the location fingerprint that concatenates multiple channels, the proposed IPS achieves a perfect centimeter localization accuracy in an NLOS environment with one pair of single-antenna WiFi devices.

## VI. DISCUSSION

### A. Achievable Localization Accuracy

In Section V, we demonstrate the centimeter-level localization accuracy of the proposed IPS with a fine-grained measurement of 5 cm resolution. In a recent experiment, we

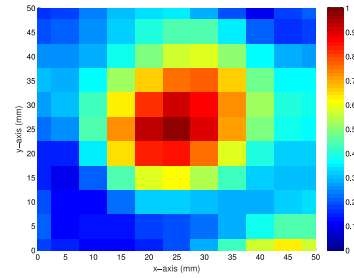


Fig. 14. TRRS near the intended location with a measurement resolution of 0.5 cm.

refine the measurement resolution to 0.5 cm to study the accuracy. The TRRS near the intended location is shown in Fig. 14 with  $W_e = 125$  MHz, which demonstrate that the localization accuracy can reach 1–2 cm in an NLOS environment.

### B. Complexity of Fingerprint Collecting

In this paper, the CFRs are collected in a 2-D space. In practice, localization of an object requires CFR measurement from a 3-D space with a centimeter-level granularity. In this case, the complexity of CFR measurement can be too high to be practical, especially for a large indoor space.

The burden of measurement can be significantly reduced since we only need to obtain the fingerprints of a limited number of areas which are more critical than the others. For instance, in an office, the main entrance and exit of the office as well as the entrance to some office rooms are of higher importance than the other areas, while in a museum, areas closer to the paintings could be more important. Fine-grained CFR measurements can be confined to these areas-of-interest. On the other hand, the efficiency of measurement can be boosted by automation techniques such as robotics.

### C. Scalability

We notice that most of the calculations in the offline phase and online phase can be interpreted as linear operations. Thus, the computational complexity of the proposed IPS scales linearly with the number of location fingerprints stored in the database. As the offline phase can in general tolerate a large delay, the increase in the computational complexity of the offline phase is less significant. On the other hand, the increase of the complexity imposes a challenge to the online phase since the online phase is much more time-sensitive than the offline phase. This issue becomes more severe when a huge number of fingerprints are stored in the database.

To deal with this problem, other information such as the sensory information or the RSSI values can be retrieved to supplement the proposed IPS with a coarse position estimation. Then, the proposed IPS can choose a subset of the fingerprints from the database that are collected nearby the estimated location to formulate a refined estimation.

### D. Fingerprint Degradation With Time

In an indoor space, movement of small and large objects such as chairs and desks should be expected. These movements

slightly changes the environment and thus introduces deviations into the CFRs collected in the offline phase. According to our most recent work in [36] and [37], we find that a large effective bandwidth can reduce the sensitivity of the fingerprints to the environmental dynamics, which can be achieved by concatenating an enough number of channels using frequency hopping.

### E. CFR Acquisition on Commercial WiFi Devices

USRPs are used as the prototype to acquire CFRs due to the fact that CFRs are unavailable on most commercial WiFi devices. More recently, the CFRs can be obtained on the off-the-shelf 802.11n device, Intel Wi-Fi Wireless Link 5300, after modification of the firmware and the wireless driver [37]. Currently, we are investigating the IPS performance using the off-the-shelf WiFi devices as well as implementing the frequency hopping mechanism.

## VII. CONCLUSION

In this paper, we present a WiFi-based IPS that exploits the frequency diversity to achieve centimeter accuracy for indoor localization. The proposed IPS fully harnesses the frequency diversity by CFR measurements on multiple channels via frequency hopping. Impacts of synchronization errors and interference are mitigated by CFR sanitization, sifting, and averaging. The averaged CFRs of different channels are then concatenated together into location fingerprints to augment the effective bandwidth. The location fingerprints are stored into a database in the offline phase and are used to calculate the TRRS in the online phase. Finally, the proposed IPS determines the location based on the TRRS. Extensive experiment results of measurements on a 1 GHz frequency band demonstrate the centimeter localization accuracy of the proposed IPS in a typical office environment with a large effective bandwidth.

## REFERENCES

- [1] J. G. McNeff, "The global positioning system," *IEEE Trans. Microw. Theory Techn.*, vol. 50, no. 3, pp. 645–652, Mar. 2002.
- [2] E. Bruns, B. Brombach, T. Zeidler, and O. Bimber, "Enabling mobile phones to support large-scale museum guidance," *IEEE MultiMedia*, vol. 14, no. 2, pp. 16–25, Apr./Jun. 2007.
- [3] S. Wang, S. Fidler, and R. Urtasun, "Lost shopping! Monocular localization in large indoor spaces," in *Proc. IEEE Int. Conf. Comput. Vis.*, Santiago, Chile, 2015, pp. 2695–2703.
- [4] Z. Yang, Z. Zhou, and Y. Liu, "From RSSI to CSI: Indoor localization via channel response," *ACM Comput. Surveys*, vol. 46, no. 2, p. 25, 2013.
- [5] J. Hightower, R. Want, and G. Borriello, "SpotON: An indoor 3D location sensing technology based on RF signal strength," Dept. Comput. Sci. Eng., Univ. Washington, Seattle, WA, USA, Tech. Rep. UW CSE 00-02-02, Feb. 2000.
- [6] L. M. Ni, Y. Liu, Y. C. Lau, and A. P. Patil, "LANDMARC: Indoor location sensing using active RFID," in *Proc. 1st IEEE Int. Conf. Pervasive Comput. Commun. (PerCom)*, Fort Worth, TX, USA, Mar. 2003, pp. 407–415.
- [7] Q. Zhang, C. H. Foh, B.-C. Seet, and A. C. M. Fong, "RSS ranging based Wi-Fi localization for unknown path loss exponent," in *Proc. IEEE Glob. Telecommun. Conf. (GLOBECOM)*, Houston, TX, USA, Dec. 2011, pp. 1–5.
- [8] B. Campbell, P. Dutta, B. Kempke, Y.-S. Kuo, and P. Pannuto, "Decawave: Exploring state of the art commercial localization," Elect. Eng. Comput. Sci. Dept., Univ. Michigan, Ann Arbor, MI, USA, Tech. Rep., 2015.
- [9] *Ubisense*. Accessed on May 26, 2016. [Online]. Available: <http://ubisense.net/>
- [10] D. Vasishth, S. Kumar, and D. Katabi, "Decimeter-level localization with a single WiFi access point," in *Proc. 13th USENIX Symp. Netw. Syst. Design Implement. (NSDI)*, Santa Clara, CA, USA, Mar. 2016, pp. 165–178.
- [11] J. Gjengset, J. Xiong, G. McPhillips, and K. Jamieson, "Phaser: Enabling phased array signal processing on commodity WiFi access points," in *Proc. 20th Annu. Int. Conf. Mobile Comput. Netw. (MobiCom)*, Maui, HI, USA, 2014, pp. 153–164.
- [12] J. Xiong and K. Jamieson, "Arraytrack: A fine-grained indoor location system," in *Proc. 10th USENIX Conf. Netw. Syst. Design Implement. (NSDI)*, Lombard, IL, USA, 2013, pp. 71–84.
- [13] P. Bahl and V. Padmanabhan, "RADAR: An in-building RF-based user location and tracking system," in *Proc. IEEE INFOCOM*, vol. 2. Tel Aviv, Israel, 2000, pp. 775–784.
- [14] M. Youssef and A. Agrawala, "The Horus WLAN location determination system," in *Proc. 3rd Int. Conf. Mobile Syst. Appl. Services (MobiSys)*, Seattle, WA, USA, 2005, pp. 205–218.
- [15] P. Prasithsangaree, P. Krishnamurthy, and P. Chrysanthis, "On indoor position location with wireless LANs," in *Proc. 13th IEEE Int. Symp. Pers. Indoor Mobile Radio Commun.*, vol. 2. Lisbon, Portugal, Sep. 2002, pp. 720–724.
- [16] C. Wu, Z. Yang, and Y. Liu, "Smartphones based crowdsourcing for indoor localization," *IEEE Trans. Mobile Comput.*, vol. 14, no. 2, pp. 444–457, Feb. 2015.
- [17] S. Sen, B. Radunovic, R. R. Choudhury, and T. Minka, "You are facing the Mona Lisa: Spot localization using PHY layer information," in *Proc. 10th Int. Conf. Mobile Syst. Appl. Services (MobiSys)*, Ambleside, U.K., 2012, pp. 183–196.
- [18] J. Xiao, K. Wu, Y. Yi, and L. M. Ni, "FIFS: Fine-grained indoor fingerprinting system," in *Proc. 21st Int. Conf. Comput. Commun. Netw. (ICCCN)*, Munich, Germany, Jul. 2012, pp. 1–7.
- [19] Y. Chapre, A. Ignjatovic, A. Seneviratne, and S. Jha, "CSI-MIMO: Indoor Wi-Fi fingerprinting system," in *Proc. IEEE 39th Conf. Local Comput. Netw. (LCN)*, Edmonton, AB, Canada, Sep. 2014, pp. 202–209.
- [20] Z.-H. Wu, Y. Han, Y. Chen, and K. J. R. Liu, "A time-reversal paradigm for indoor positioning system," *IEEE Trans. Veh. Technol.*, vol. 64, no. 4, pp. 1331–1339, Apr. 2015.
- [21] C. Chen, Y. Chen, H.-Q. Lai, Y. Han, and K. J. R. Liu, "High accuracy indoor localization: A WiFi-based approach," in *Proc. IEEE Int. Conf. Acoust. Speech Signal Process. (ICASSP)*, Shanghai, China, Mar. 2016, pp. 6245–6249.
- [22] B. Wang, Y. Wu, F. Han, Y.-H. Yang, and K. J. R. Liu, "Green wireless communications: A time-reversal paradigm," *IEEE J. Sel. Areas Commun.*, vol. 29, no. 8, pp. 1698–1710, Sep. 2011.
- [23] M. Fink, "Acoustic time-reversal mirrors," in *Imaging of Complex Media With Acoustic and Seismic Waves* (Topics in Applied Physics), vol. 84, M. Fink, W. A. Kuperman, J.-P. Montagner, and A. Tourin, Eds. Heidelberg, Germany: Springer, 2002.
- [24] M. Fink, C. Prada, F. Wu, and D. Cassereau, "Self focusing in inhomogeneous media with time reversal acoustic mirrors," in *Proc. IEEE Ultrason. Symp.*, vol. 2. Montreal, QC, Canada, Oct. 1989, pp. 681–686.
- [25] C. Dorme, M. Fink, and C. Prada, "Focusing in transmit-receive mode through inhomogeneous media: The matched filter approach," in *Proc. IEEE Ultrason. Symp.*, vol. 1. Tucson, AZ, USA, Oct. 1992, pp. 629–634.
- [26] F. Han, Y.-H. Yang, B. Wang, Y. Wu, and K. J. R. Liu, "Time-reversal division multiple access over multi-path channels," *IEEE Trans. Commun.*, vol. 60, no. 7, pp. 1953–1965, Jul. 2012.
- [27] J. Heiskala and J. Terry, *OFDM Wireless LANs: A Theoretical and Practical Guide*. Indianapolis, IN, USA: Sams, 2001.
- [28] T.-D. Chiueh and P.-Y. Tsai, *OFDM Baseband Receiver Design for Wireless Communications*. New York, NY, USA: Wiley, 2007.
- [29] M. Speth, S. A. Fechtel, G. Fock, and H. Meyr, "Optimum receiver design for wireless broad-band systems using OFDM—Part I," *IEEE Trans. Commun.*, vol. 47, no. 11, pp. 1668–1677, Nov. 1999.
- [30] I. W. Group et al., *Supplement to IEEE Standard for Information Technology Telecommunications and Information Exchange Between Systems Local and Metropolitan Area Networks, Specific Requirements, Part 11: Wireless LAN Medium Access Control (MAC) and Physical Layer (PHY) Specifications: High-Speed Physical Layer in the 5 GHz Band*, IEEE Standard 802.11a-1999, 1999.
- [31] A. V. Oppenheim, R. W. Schaffer, and J. R. Buck, *Discrete-Time Signal Processing*, 2nd ed. Upper Saddle River, NJ, USA: Prentice-Hall, 1999.

- [32] M. Speth, S. Fechtel, G. Fock, and H. Meyr, "Optimum receiver design for OFDM-based broadband transmission II. A case study," *IEEE Trans. Commun.*, vol. 49, no. 4, pp. 571–578, Apr. 2001.
- [33] *Ettus Research LLC*. Accessed on May 26, 2016. [Online]. Available: <http://www.ettus.com/>
- [34] B. Bloessl, M. Segata, C. Sommer, and F. Dressler, "Decoding IEEE 802.11a/g/p OFDM in Software using GNU Radio," in *Proc. 19th ACM Int. Conf. Mobile Comput. Netw. (MobiCom)*, Miami, FL, USA, Oct. 2013, pp. 159–161.
- [35] *GNU Radio*. Accessed on May 26, 2016. [Online]. Available: <http://gnuradio.org/>
- [36] C. Chen, Y. Chen, Y. Han, H. Lai, F. Zhang, and K. J. R. Liu, "Achieving centimeter accuracy indoor localization on WiFi platforms: An multi-antenna approach," *IEEE Internet Things J.*, vol. 4, no. 1, pp. 122–134, Feb. 2017.
- [37] C. Chen, Y. Han, Y. Chen, and K. J. R. Liu, "Indoor global positioning system with centimeter accuracy using Wi-Fi [applications corner]," *IEEE Signal Process. Mag.*, vol. 33, no. 6, pp. 128–134, Nov. 2016.



**Chen Chen** (S'15) received the B.S. and M.S. degrees from the Department of Microelectronics, Fudan University, Shanghai, China, in 2010 and 2013, respectively. He is currently pursuing the Ph.D. degree at the Department of Electrical and Computer Engineering, University of Maryland at College Park, College Park, MD, USA.

His current research interests include biomedical signal processing, indoor localization, and wireless communications.

Mr. Chen was a recipient of multiple honors and awards, including the Best Student Paper Award at the IEEE ICASSP 2016, the Litton Industries Fellowship from University of Maryland at College Park, in 2015, the Distinguished Graduate Student Teaching Award from the University of Maryland at College Park, in 2014, and the Excellent Graduate Student of Shanghai in 2013.



**Yan Chen** (SM'14) received the B.S. degree from the University of Science and Technology of China, Hefei, China, in 2004, the M.Phil. degree from the Hong Kong University of Science and Technology, Hong Kong, in 2007, and the Ph.D. degree from the University of Maryland at College Park, College Park, MD, USA, in 2011.

Being a Founding Member, he joined Origin Wireless Inc., Greenbelt, MD, USA, in 2013, as a Principal Technologist. He is currently a Professor with the University of Electronic Science and

Technology of China, Chengdu, China. His current research interests include multimedia, signal processing, game theory, and wireless communications.

Dr. Chen was a recipient of multiple honors and awards, including the Best Student Paper Award at the IEEE ICASSP in 2016, the Best Paper Award at the IEEE GLOBECOM in 2013, the Future Faculty Fellowship and the Distinguished Dissertation Fellowship Honorable Mention from the Department of Electrical and Computer Engineering in 2010 and 2011, the Finalist of the Dean's Doctoral Research Award from the A. James Clark School of Engineering, the University of Maryland in 2011, and the Chinese Government Award for Outstanding Students Abroad in 2010.



**Yi Han** (GS'14–M'15) received the B.S. (Hons.) degree in electrical engineering from Zhejiang University, Hangzhou, China, in 2011, and the Ph.D. degree from the Department of Electrical and Computer Engineering, University of Maryland at College Park, College Park, MD, USA.

He is currently the Wireless Architect with Origin Wireless Inc., Greenbelt, MD, USA. His current research interests include wireless communication and signal processing.

Dr. Han was a recipient of the Best Student Paper Award at the IEEE ICASSP in 2016 and Class A Scholarship from Chu Kochen Honors College, Zhejiang University, in 2008.



**Hung-Quoc Lai** (M'11) received the B.S. (*cum laude*), M.S., and Ph.D. degrees from the University of Maryland at College Park, College Park, MD, USA, in 2004, 2006, and 2011, respectively, all in electrical engineering.

In 2013, he joined Origin Wireless, Greenbelt, MD, USA, where he is a Founding Member and currently the Vice President of Engineering, which develops advanced time reversal wireless technologies for use in a wide variety of applications of indoor positioning/tracking, monitoring, security,

radio human biometrics, wireless power transfer, and 5G communications. He was a Technical Lead in research and development of multiple-input multiple-output and cooperative communications with the U.S. Army RDECOM CERDEC, Aberdeen Proving Ground, MD, USA. He is a Gates Millennium Scholar.



**K. J. Ray Liu** (F'03) was a Distinguished Scholar-Teacher of the University of Maryland at College Park, College Park, MD, USA, in 2007, where he is a Christine Kim Eminent Professor of Information Technology. He leads the Maryland Signals and Information Group conducting research encompassing broad areas of information and communications technology with recent focus on smart radios for smart life.

Dr. Liu is a Fellow of the AAAS. He was a recipient of the 2016 IEEE Leon K. Kirchmayer Technical Field Award on graduate teaching and mentoring, the IEEE Signal Processing Society 2014 Society Award, the IEEE Signal Processing Society 2009 Technical Achievement Award, the Highly Cited Researcher Award by Thomson Reuters, the teaching and research recognitions from the University of Maryland, including the University-Level Invention of the Year Award and the College-Level Poole and Kent Senior Faculty Teaching Award, the Outstanding Faculty Research Award, and the Outstanding Faculty Service Award, all from A. James Clark School of Engineering. He is a member of IEEE Board of Director. He was the President of the IEEE Signal Processing Society, where he has served as Vice President—Publications and Board of Governor. He has also served as the Editor-in-Chief of the *IEEE Signal Processing Magazine*.